APPENDIX A

NUMERICAL SIMULATION OF STRONG GROUND MOTION USING THE STOCHASTIC GROUND MOTION MODEL FOR SUBDUCTION EARTHQUAKES

Introduction

The estimation of strong ground motion, particularly at close distances to large magnitude earthquakes is a difficult task. Until recently, only empirical approaches could be reliably used to specify median values and to provide estimates of uncertainty. Early numerical methods were notoriously cumbersome and highly dependent upon a large number of poorly characterized parameters. As a result, ground motion predictions based on these numerical modeling techniques suffered from generally poor and unquantified reliability. Due to computational limitations, results based on these methods were generally non site-specific such that the effects of the shallow crustal properties as well as soil profiles were not directly modeled. In addition, as a result of being highly sensitive to poorly known parameters as well as having large computational demands, the uncertainties of predicted motions due to parameter uncertainties and possible model bias were left largely unquantified.

Recently however, a new ground motion model has been introduced that characterizes strong ground motions as stochastic in time, with a Fourier amplitude spectrum specified by a fundamentally simple and deterministic seismological model of the source, path, and site (Hanks and McGuire, 1981; Boore, 1983,1986; Silva, 1991). An essential and significant aspect of the new model is that, while being extremely simple, it also provides estimates of strong ground motions with remarkable accuracy. Additional, but important, side benefits arising from the model's simplicity are the natural separation of source, path, and site effects and the accompanying computational efficiency. As a result, an accurate appraisal of the effects of uncertainties in source, path, and site parameters as well as any model bias can be readily quantified.

Point Source Ground Motion Model

The stochastic ground motion model (sometimes referred to as the Band-Limited-White-Noise or BLWN model), in which the energy is distributed randomly over the duration of the source, has proven remarkably effective in correlating with a wide range of ground motion observations. Time-domain measures such as peak acceleration and peak particle velocity, Wood-Anderson magnitude, and short-period P- and S-wave amplitudes as well as frequency-domain measures such as relative velocity response and Fourier amplitude spectra, have been predicted with reasonable accuracy (Hanks and McGuire, 1981; Boore, 1983, 1986; Boore and Atkinson, 1987; Silva and Lee, 1987; Toro and McGuire, 1987; Silva and Darragh, 1992). The ground motion model employed here uses an ω-square Brune source model (Brune, 1970; 1971) with a single corner frequency and a constant stress drop (Boore, 1983; Atkinson, 1984) (Figure 1).

The acceleration spectral density a(f), where f is frequency, is given by

$$a(f) = C \frac{f^2}{1+(f/f_c)^2} \frac{M0}{R} P(f) A(f) e^{-\frac{\pi f R}{\beta_0 Q(f)}} \quad (1)$$

where

M_o = Seismic moment

R = Distance to the equivalent point source

β_o = Shear-wave velocity at the source

$Q(f)$ = $Q_o f^{\eta}$, frequency-dependent quality factor model where Q_o and η are model parameters

$A(f)$ = Near-surface amplification factors

$P(f)$ = High-frequency truncation filter

f_c = Source corner frequency and

C = $(1/\rho_o\beta_o^3)$ x (2) x (0.55) x $(1/\sqrt{2})$ x π.

C is a constant which contains source-region density ρ_o and shear-wave velocity terms and accounts for the free-surface effect (factor of 2), the source radiation pattern averaged over a sphere (0.55) (Boore, 1986), and the partition of energy into two horizontal components ($1/\sqrt{2}$)

Source scaling is provided by specifying two independent parameters, the seismic moment (M_o) and the stress drop ($\Delta\sigma$) (Figure 1). The seismic moment is related to magnitude through the definition of moment magnitude M by the relation

$$\log M_0 = 1.5\ M + 16.1 \qquad \text{(Hanks and Kanamori, 1979)} \qquad (2).$$

The stress drop $\Delta\sigma$ relates the corner frequency f_c to M_0 through the relation

$$f_c = \beta_o\ (\Delta\sigma/8.44\ M_o)^{1/3} \qquad \text{(Brune, 1970; 1971)} \qquad (3).$$

The spectral shape of the single-corner-frequency ω-square source model is then described by the two free parameters M_o and $\Delta\sigma$. The corner frequency increases with the shear-wave velocity and with increasing stress drop, both of which may be region dependent.

In order to compute peak time-domain values, i.e. peak acceleration, peak particle velocity, and peak oscillator response, random vibration theory (RVT) is used to relate RMS calculations to peak value estimates (Boore, 1983; Boore and Joyner, 1984).

Point Source Model Parameters

In a half-space model, the near-surface amplification factors, A(f), account for the increase in amplitude as the seismic energy travels through lower-velocity crustal materials near the surface (Figure 1) (Boore, 1986; Silva and Darragh, 1995). These factors depend on average crustal and near-surface shear-wave velocity and density. The P(f) filter models the observation that acceleration spectral density appears to fall off rapidly beyond some region-dependent maximum frequency. This observed phenomenon truncates the high-frequency portion of the spectrum and is responsible for the band-limited nature of the stochastic model. This spectral fall-off has been attributed to near-site attenuation (Hanks, 1982; Anderson and Hough, 1984) or to source processes (Papageorgiou and Aki, 1983) or perhaps to both effects. Hanks (1982) termed the phrase f_{max} to describe this site-dependent corner frequency. In the Anderson and Hough (1984) attenuation model, which is adopted in this study, the form of the P(f) filter is taken as

$$P(f) = e^{-\pi\kappa(0)f} \qquad (4).$$

$\kappa(0)$ is a site- and distance-dependent parameter (here taken at r=0) that represents the effect of intrinsic attenuation on the seismic waves as they propagate through the crust from source to receiver (Figure 1). Kappa depends on epicentral distance (r) and on both the shear-wave velocity (β_R) and quality factor (Q_s) averaged over a depth of H beneath the receiver or site. At zero epicentral distance, κ is given by

$$\kappa(0) = \frac{H}{\overline{\beta_R}\,\overline{Q_s}} \qquad (5)$$

The value of $\kappa(0)$ is attributed to attenuation in the very shallow crust directly beneath the site (Hough and Anderson, 1988). Silva and Darragh (1995) suggest that the

predominant kappa effects extend from the surface down to several hundred meters and possibly as deep as 1 to 2 km. The intrinsic attenuation along this part of the path is thought to be frequency-independent, but site-dependent (Hough et al., 1988). Kappa has been determined for several rock and soil sites representative of western North America (WNA) (Anderson and Hough, 1984; Anderson, 1986). For an average WNA rock site, a value between 0.02 and 0.06 sec is appropriate (Boore, 1986; Silva and Darragh, 1995). For eastern North America, a stable continental interior with generally older and stronger crustal rocks, average kappa values range from about 0.004 sec to about 0.01 sec (Silva and Darragh, 1995).

The crustal anelastic attenuation from the source to just below the site is modeled with the frequency-dependent quality factors $Q(f)$. Geometrical attenuation is taken as 1/R (or $1/\sqrt{R}$ for distances greater than about 100 km). In order to accommodate the effects of direct and supercritically-reflected waves in a crustal structure, this simple geometrical attenuation can be replaced by a formulation due to Ou and Herrmann (1990). With this technique, the geometrical attenuation and duration for direct plus post-critical reflections may be computed in a manner appropriate to the BLWN-RVT model.

The Fourier amplitude spectrum, $a(f)$, models direct shear waves in a homogeneous half-space (with effects of a velocity gradient through the $A(f)$ transfer function). For vertically heterogenous layered structures, the plane-wave propagators of Silva (1976) are used to propagate SH or P-SV motion through the layered structure.

To model an average horizontal component, the computed Fourier amplitude spectrum (Equation 1) is input as outcrop motion at the top of the source layer using the SH propagators. Normal incidence is assumed and the crust is taken as elastic with damping accommodated in the $Q(f)$ and kappa factors.

For fixed magnitude (moment) and distance, specific source, path, and site parameters are stress drop ($\Delta\sigma$), crustal damping ($Q(f)$), crustal shear-wave velocity profile, and kappa (κ). These represent the point-source ground-motion parameters for a rock site.

Finite Source Model Ground Motion Model

In the near-source region of large earthquakes, aspects of a finite source including rupture propagation, directivity, and source-receiver geometry can be significant and may be incorporated into strong ground motion predictions. To accommodate these effects, a methodology that combines the aspects of finite-earthquake-source modeling techniques (Hartzell, 1978) with the BLWN-RVT point-source ground motion model has been developed to produce response spectra as well as time histories appropriate for engineering design (Silva et al., 1990; Silva and Stark, 1992; Schneider et al., 1993; Beresnev and Atkinson, 1997; Silva et al., 1997). The approach is very similar to the empirical Green function methodology introduced by Hartzell (1978) and Irikura (1983). In this case however, the stochastic point source is substituted for the empirical Green function and peak amplitudes; PGA, PGV, and response spectra (when time histories are not produced) are estimated using random process theory. Use of the stochastic point source as a Green function is motivated by its demonstrated success in modeling ground motions in general and particularly strong ground motions (Boore, 1983, 1986; Silva and Stark, 1992; Schneider et al., 1993) and the desire to have a model that is truly site and region specific. The model can accommodate a region specific Q(f), Green function sources of arbitrary moment or stress drop, and site specific kappa values. The necessity of regional and site specific recordings or the modification of possibly inappropriate empirical Green functions is eliminated.

For the finite-source characterization, a rectangular fault is discretized to provide the locations of NS subfaults of moment M_0^S. The empirical relationship

$$M = 4.02 + \log A \qquad \text{(Wells and Coppersmith, 1993)} \qquad (6)$$

is used to assign areas to both the target earthquake (if its rupture surface is not fixed) as well as to the subfaults. The subevent magnitude M^S is generally taken in the range of 5.0-6.5 depending upon the size of the target event. The value of NS is determined as the

ratio of the target event area to the subfault area. To constrain the proper moment, the total number of events summed (N) is given by the ratio of the target event moment to the subevent moment. The subevent rise time is determined by the equation

$$\log \tau_S = 0.33 \log M_o^S - 8.62 \qquad (7)$$

which results from a fit to the M_0 - rise time data listed in Heaton (1990). Slip on each subfault continues for a time τ_S times N/NS which is the modeled or target event rise time. Heterogeneity of the earthquake source process is modeled by randomizing the location of the sub-events within each subfault (Hartzell, 1978) as well as the subevent rise time. The stress drop of the stochastic point-source Green function is taken as

$$\Delta\sigma = \frac{7}{16}\left(\frac{M_e}{R_e^3}\right) \qquad (8).$$

where R_e is the equivalent circular radius of the rectangular sub-event.

Different values of slip are assigned to each subfault as relative weights so that asperities or non-uniform slip can be incorporated into the methodology. The rupture velocity is taken as depth independent at a value of 0.8 times the shear-wave velocity generally at the half-depth of the slip surface. A random component (20%) is added to the rupture velocity. The radiation pattern is computed for each subfault, a random component added, and the RMS applied to the motions computed at the site.

The ground-motion time history at the receiver is computed by summing the contributions from each subfault associated with the closest Green function, transforming to the frequency domain, and convolving with the Green function spectrum (Equation 1). The locations of the Green functions are generally taken at center of each subfault for small subfaults or at a maximum separation of about 5-10 km for large subfaults. As a final step, the individual contributions associated with each Green function are summed in the frequency domain multiplied by the RMS radiation pattern, and the resultant power spectrum at the site is computed. The appropriate duration used in the RVT

computations for PGA, PGV, and oscillator response is computed by transforming the summed Fourier spectrum into the time domain and computing the 5-75% arias intensity (Ou and Herrmann, 1990).

As with the point-source model, crustal response effects are accommodated through the amplification factor (A(f)) or by using vertically propagating shear waves through a vertically heterogenous crustal structure. Propagation path damping, through the Q(f) model, is incorporated from each fault element to the site. Near-surface crustal damping is incorporated through the kappa operator (Equation 1). To model crustal propagation path effects, the method of Ou and Herrmann (1990) can be applied from each subfault to the site.

Time histories may be computed in the process as well by simply adding a phase spectrum appropriate to the subevent earthquake. The phase spectrum can be extracted from a recording made at close distance to an earthquake of a size comparable to that of the subevent (generally M 5.0-6.5). Interestingly, the phase spectrum need not be from a recording in the region of interest. A recording in WNA can effectively be used to simulate motions appropriate to ENA (Silva et al., 1989). Transforming the Fourier spectrum computed at the site into the time domain results in a computed time history which includes all of the aspects of rupture propagation, source finiteness, as well as propagation path and site effects.

For fixed fault size, mechanism, and moment, the specific source parameters for the finite fault are slip distribution, location of nucleation point, and site azimuth. The propagation path and site parameters remain identical for both the point- and finite- source models.

Effects of Surficial Soils

The effects of a soil column upon strong ground motion have been well documented and studied analytically for many years. Wood (1908) and Reid (1910), using apparent intensity of shaking and distribution of damage from the 1906 San Francisco earthquake,

gave evidence that the severity of shaking can be substantially affected by the local geology and soil conditions. Gutenberg (1957) developed amplification factors representing different site geology by examining recordings of microseisms and earthquakes from instruments located on various types of ground. More recently, Borcherdt and Gibbs (1976), Seed et al. (1969), Wiggins (1964), Idriss and Seed (1968), Berill (1977), Joyner et al. (1976), Duke and Mal (1978), Silva (1991), and Silva and Stark (1992) have shown that during small and large earthquakes, the surface soil motion can differ in significant and predictable ways from that on adjacent rock outcrops. In addition, other investigators have utilized explosion data either independently or in conjunction with earthquake data to examine site response characteristics (Murphy et al., 1971; Rogers et al., 1984; and Hays et al., 1979). Recent work using horizontal as well as vertical arrays of instruments have demonstrated the general consistency of the site response for seismic events of different sizes, distances, and azimuths (Tucker and King, 1984; Benites et al., 1985).

Results of these and other studies have demonstrated, in a general sense, the adequacy of assuming plane-wave propagation in modeling one-dimensional site response for engineering purposes. The simple model then represents a useful analytical tool to approximate site effects on strong ground motion.

To model soil response, an RVT-based equivalent-linear approach is used by propagating either the point- or finite-source outcrop power spectral density through a one-dimensional soil column. RVT is used to predict peak time domain values of shear-strain based upon the shear-strain power spectrum. In this sense, the procedure is analogous to the program SHAKE (Schnabel et al., 1972) except that peak shear strains in SHAKE are measured in the time domain. The purely frequency domain approach obviates a time domain control motion and, perhaps just as significantly, eliminates the need for a suite of analyses based on different input motions. This arises because each time domain analysis may be viewed as one realization of a random process. In this case, several realizations of the random process must be sampled to have a statistically stable estimate of site response. The realizations are usually performed by employing different control

motions with approximately the same level of peak acceleration. In the frequency-domain approach, the estimates of peak shear strain as well as oscillator response are, as a result of the RVT, fundamentally probabilistic in nature. Stable estimates of site response can then be rapidly computed permitting statistically significant estimates of uncertainties based on parametric variations.

The parameters that influence computed response include the shear-wave velocity profile and the strain dependencies of both the shear modulus and shear-wave damping.

Finite Source Model Uncertainties

An important aspect of any numerical modeling approach is a proper statistical estimate of uncertainty. Modeling uncertainty is basically a goodness-of-fit test using given model parameter values. The combination of parametric uncertainty (the variation in computed response due to a variation in parameters) and modeling uncertainty represents the total uncertainty in the ground motion prediction.

A quantitative assessment of the modeling uncertainty (Abrahamson et al., 1990) associated with both the finite-fault RVT numerical predictions has been computed for the 1985 Michoacan, Mexico and 1985 Valpariso, Chile earthquakes as well as 15 crustal earthquakes at about 500 sites (Silva et al., 1997). For Michoacan earthquake, strong ground motions recorded at 14 rock sites in the epicentral distance range of 20-400 km were modeled using the stochastic finite-fault RVT model (Silva and Stark, 1992). For the Valpariso, Chile earthquake 6 rock sites were modeled.

Michoacan, Mexico Simulations

Source model

Figure 2 shows a map of central Mexico along with epicenters and aftershock zones of large earthquakes which occurred in the region since 1951. The aftershock zone of the

September 19, 1985 earthquake is outlined in long dashed lines with PGA values recorded at the Guerrero acceleragraph array are shown in parenthesis. The slip model used in the Michoacan simulations is taken from Mendez and Anderson (1991) and approximates the aftershock zone shown in Figure 2. This model is preferred over the slip distribution of Mendoza and Hartzel (1989) because it more closely matches the area outlined by the aftershocks. The Mendez and Anderson (1991) slip model is 80 km wide and 180 km long with a seismic moment of 1.4×10^{28} dyne-cm (M 8.03) and is shown in Figure 3. Magnitude 6.2 (2.6×10^{25} dyne-cm) subevents are used on subfaults with lengths and widths of 15 and 10 km resulting in 12 elements along strike and 8 along dip. The total number of events summed is given by the moment ratio of the target event (1.4×10^{28} dyne-cm) to the subevent moment (2.6×10^{25} dyne-cm) or about 538. Since 96 subfaults are used to cover the slip surface, each element is taken to rupture for a duration of 3.6 seconds; 6 times the subevent rise time of 0.6 sec (Equation 7).

Path Model

Geometrical attenuation is taken as 1/R for subfault to site distances less than 100 km and 1/SQRT(R) otherwise. The Q(f) model was determined by Humphrey and Anderson (1993) by inverting strong motion data recorded at the Guesrero array from about 30 earthquakes. The model is given by $273\ f^{0.66}$. The crustal velocity model, used only to compute vertical propagating shear-wave amplification assuming an average source depth of 15 km, is taken from Somerville et al. (1991).

Site Model

Fourteen rock sites of the Guerrero array covering the rupture surface-to-site distance range of about 15 to 250 km are modeled. Kappa values are available for all of the sites as well as amplification factors for several of the sites from independent studies (Silva and Darragh, 1995; Humphrey and Anderson, 1993). Table 1 lists the site names, labels, and kappa values and also indicates which sites have frequency dependent site factors. The kappa values determined by Silva and Darragh (1995) are based on template fits to

response spectral shapes for several earthquakes while the kappa values and site factors determined by Humphrey and Anderson (1993) are a result of fits to Fourier amplitude spectra using 30 earthquakes. Figure 4 shows the Humphrey and Anderson site terms available for the modeled sites which are plotted over the bandwidths considered reliable for each site. Only those site terms with 3 or more recordings (and not including the Michoacan main shock) are used. The site terms represent unmodeled site amplifications and deamplification due to crustal heterogeneities and perhaps topographic effects. The values are near 1 on average and can vary by factors of 5 or more with frequency.

Michoacan Modeling Uncertainty

Comparisons of 5% damped spectral acceleration computed for the 1985 M 8.03 Michoacan main shock to the log average of the two horizontal components computed from the recordings are shown in Figure 5. Included in the simulations are the site specific kappa values (Table 1) as well as the site factors of Humphrey and Anderson (1993) (Figure 4). For most of the sites, there is good agreement between recorded motions and computed motions from PGA values at 0.02 sec out to 10-20 sec. At the closest sites: CMP, VIL, UNI, and ZIH model predictions generally exceed recorded motions. While for the more distant sites, the agreement is closer. Overall the model predicts the recorded motions very well considering its simplicity in that no computationally intensive wave propagation calculations were performed and a simple theoretical single-corner-frequency constant-stress-drop set of Green functions were used.

To provide a quantative measure of the uncertainties in the ground-motion predictions, a simple goodness-of-fit was performed at each spectral period. The difference of the logarithms of the observed average 5%-damped acceleration response spectra and the predicted response spectra were calculated at each period, squared, and summed over the total number of sites (14 sites). Dividing the resultant by the number of sites (assuming zero bias) results in an estimate of the model variance or uncertainty (Abrahamson et al., 1990). Figure 6 shows the computed standard error (σ_{ln}) verses frequency from 0.01 Hz

to 50 Hz as well as the computed model bias (Abrahamson et al., 1990). Over the frequency range of interest, 1-30 Hz, the uncertainty is quite low, with an average about 0.35-0.40, indicating an accurate prediction of the recorded motions. For frequencies below about 0.5 Hz, the uncertainty rises sharply to an average level of about 0.75. The increase in uncertainty at low frequencies is the result of a general overprediction of the ground motions and is reflected in the negative bias values. In general however, the simple model gives an accurate prediction of the recorded motions over a surprisingly wide bandwidth and shows zero bias (90% confidence limits) from 50-0.5 Hz.

To examine the effect of modeling direct plus post-critically reflected waves from each subfault to the site, the method of Ou and Herrmann (1990) was incorporated into the methodology. The results are shown in Figure 7 for response spectra and Figure 8 for the uncertainty and bias using the same model parameters. Interestingly, the improvement in fit is most significant at low frequencies (about 0.1-0.5 Hz) with a slight reduction in uncertainty at high frequencies. For frequencies above 0.5 Hz, this result is very good news for strong ground motion prediction since it suggests that an accurate and detailed crustal model does not significantly improve the accuracy of the simulated motions. Apparently, over this frequency range, the recorded strong ground motions are largely stochastic in nature and random source processes as well as non-uniform vertical and lateral variations in crustal properties results in significant departures from detailed deterministic model predictions. Simply using 1/R (1/SQRT(R) for R>100 km) works about as well as detailed wave propagation modeling, relaxes the dependence on an accurate crustal model as well as the possibility of simulating inaccurate motions if the crustal model is incorrect. The simple geometrical attenuation also is a lot easier and more cost effective to implement.

To examine the effects of site specific kappa values as well as the 6 site functions, two additional analyses were performed. Model uncertainties were computed for simulations using site specific kappa values only (no site factors) as well as using simply an average kappa value of 0.042 sec (mean of the site specific values), again with no site factors. The results are shown in Figures 9. Eliminating the site factors only, retaining site

specific kappa terms, results in a dramatic increase in uncertainty for frequencies above about 2-3 Hz to an average value of about 0.5, an increase of over 60%. Replacing the site dependent kappa values with a constant of 0.042 sec further increases the uncertainty but for frequencies exceeding about 4 Hz. Interesting, although the site terms are considered stable and reliable for frequencies below 2-3 Hz they offer no apparent reduction in uncertainty and only slightly improve the bias estimates at low frequencies (Figure 9).

In terms of model predictions, these results indicate that for rock sites with kappa values in the range sampled (0.02 to about 0.10 sec with a mean of 0.042 sec) knowledge of site kappa can reduce uncertainty by a significant amount for frequencies above about 4 Hz. Additionally, assuming the contributions to the site terms at high frequencies are due to local shallow velocity profiles, it may be possible to further improve the accuracy of model predictions at rock sites with knowledge of the velocity profile.

In computing the final model uncertainty and bias estimates both the Michoacan, Mexico and Valpariso, Chile modeling results will be combined. For the Michoacan computations, only site specific kappa values will be included. The site factors are not included in computing the modeling uncertainty since neither an appropriate site factor is available for the site under study nor is site amplification treated in the parametric variations.

Valpariso, Chile Simulations

Source Model

For the March 3, 1985 Valpariso, Chile earthquake, little is known about the details of the slip model. Fewer free field strong motion sites are available and the site characteristics are much less well known than is the case for the Michoacan, Mexico earthquake. Somerville et al. (1990) have derived a slip model by perturbing the teleseismic model of Houston (1987) to improve the fit to the strong motion data. That slip model is adopted

for use here and is shown in Figure 11 along with the sites used in the modeling exercise. The rupture surface is 80 km wide and 210 km long with a seismic moment of 1.0 x 10^{28} dyne-cm (M 7.93) (Somerville et al., 1990). As with the Michoacan modeling, M 6.2 subevents are used with lengths and widths of 15 km and 10 km respectively. This results in 14 elements along strike and 8 along dip. The total number of events summed is 1.0 x 10^{28} dyne-cm/2.6 x 10^{25} dyne-cm or about 385. There are a total of 112 subfaults (8 x 14), each element then ruptures for a duration of 1.8 sec; 3 times the subevent rise time of 0.6 sec.

Path Model

Geometrical attenuation is taken as 1/R (1/SQRT(R) for R>100 km) for subfault to site distances. Results from the Michoacan modeling, as well as modeling of the 1987 Loma Prieta earthquake; Silva and stark (1992), suggested that this simple approach provided as good a fit to recorded strong ground motions at intermediate to high frequencies (>0.5 Hz) as approaches which incorporate detailed wave propagation models. In this case these results are significant since the crustal structure is poorly known in this region.

To include crustal amplification, the near-surface amplification factors (A(f); Boore, 1986) discussed earlier are used. These factors are appropriate for a generic western North America or tectonically active crustal province. The WNA factors are shown in Figure 11 compared to those computed for the Michoachan earthquake moldeling. The WNA amplification factors are higher at high frequencies reflecting the large near-surface velocity gradient typical of soft-rock crustal areas (Boore, 1986).

In addition to the crustal structure, the appropriate crustal damping model (Q(f)) is also poorly constrained. As a result, the Michoacan Q(f) model (273 $f^{0.66}$) is adopted. To be consistent with treating crustal damping in parametric variations, the Q(f) model should be varied to minimize the modeling uncertainty. However, since the slip model is likely poorly constrained as well, it makes little sense compensating the misfit by varying the Q(f) model.

Site Model

Six rock sites are modeled (Figure 11) since very little is known about the site specific profiles at the soil sites. Site specific kappa values were determined using templates of response spectral shapes (Silva and Darragh, 1995) and are listed on Table 2.

Valpariso Modeling Uncertainty

Computed 5% damped acceleration response spectra for the six rock sites are shown in Figure 12 compared to recorded motions. At high to intermediate frequencies (50 Hz-1 Hz), the match is good, again considering the simplicity of the model and, in this case, poorly constrained slip distribution as well as crustal damping model. Figure 13 shows the resulting modeling uncertainty and bias estimates. The low frequency range is probably limited to about 0.25 Hz since the accelerographs have film recorders. In general, the uncertainty is quite low above about 0.7 Hz and extremely low at high frequencies (above 10 Hz). The bias estimates are essentially zero (90% confidence limits) above about 0.7 Hz. Of significance, any departure of the bias estimates from zero is negative indicating an overprediction. As a result, one can then reasonably use the bias estimates to correct the model uncertainty.

Total Modeling Uncertainty

Combining the simulations for both the Michoacan, Mexico and Valpariso, Chile earthquakes results in the total modeling uncertainty. Both the uncertainty and bias estimates are shown in Figure 14. The total modeling uncertainty is quite low, generally below about 0.4 for frequencies above about 1 Hz with a small peak near 1 Hz. Above 0.6 Hz, the bias correction is essentially zero and is reflected in the near zero bias estimates above about 0.5-0.6 Hz. Over this frequency range (0.5-50 Hz), the simple model using a Brune omega-square point-source as a Green function coupled with 1/R and 1/SQRT (R) geometrical attenuation provides accurate predictions of strong ground motions from large subduction earthquakes.

REFERENCES

Abrahamson, N.A., Somerville, P.G., Cornell, C.A. (1990). "Uncertainty in numerical strong motion predictions" *Proc. Fourth U.S. Nat. Conf. Earth. Engin.*, Palm Springs, CA., 1, 407-416.

Anderson, J.G., Bodin, P., Brune, J.N., Prince, J., Singh, S.K., Quaas, R., and Onate, M. (1986). "Strong ground motion from the Michoacan, Mexico, earthquake." *Science.* 223, 1043-1049.

Anderson, J.G., and Hough, S.E. (1984). "A model for the shape of the Fourier amplitude spectrum of acceleration at high frequencies." *Bull. Seism. Soc. Am.*, 74, 1969-1993.

Atkinson, G.M. (1984). "Attenuation of strong ground motion in Canada from a random vibrations approach." *Bull. Seism. Soc. Am.*, 74(5), 2629-2653.

Benites, R., Silva, W.J., and Tucker, B. (1985). "Measurements of ground response to weak motion in La Molina Valley, Lima, Peru. Correlation with strong ground motion." *Earthquake Notes, Eastern Section, Bull. Seism. Soc. of Am.*, 55(1).

Beresnev, I.A. and G. M. Atkinson (1997). "Modeling finite-fault radiation from the ω" spectrum." *Bull. Seism. Soc. Am.,* 87(1), 67-84.

Berrill, J.B. (1977). "Site effects during the San Fernando, California, earthquake." *Proc. Sixth World Conf. on Earthquake Engin.,* India, 432-438.

Boore, D.M., and Atkinson, G.M. (1987). "Stochastic prediction of ground motion and spectral response parameters at hard-rock sites in eastern North America." *Bull. Seism. Soc. Am.*, 77(2), 440-467.

Boore, D.M. (1986). "Short-period P- and S-wave radiation from large earthquakes: implications for spectral scaling relations." *Bull. Seism. Soc. Am.*, 76(1) 43-64.

Boore, D.M. and Joyner, W.B. (1984). "A note on the use of random vibration theory to predict peak amplitudes of transient signals." *Bull. Seism. Soc. Am.*, 74, 2035-2039.

Boore, D.M. (1983). "Stochastic simulation of high-frequency ground motions based on seismological models of the radiated spectra." *Bull. Seism. Soc. Am.*, 73, 1865-1894.

Borcherdt, R.D., and Gibbs, J.F. (1976). "Effects of local geologic conditions in the San Francisco Bay region on ground motions and the intensities of the 1906 earthquake." *Bull. Seism. Soc. Am.*, 66, 467-500.

Brune, J.N. (1971). "Correction." *J. Geophys. Res.* 76, 5002.

Brune, J.N. (1970). "Tectonic stress and the spectra of seismic shear waves from earthquakes." *J. Geophys. Res.* 75, 4997-5009.

Duke, C.M., and Mal, A.K. (1978). *Site and Source Effects on Earthquake Ground Motion.* Univ. of Calif. Los Angeles Engin. Rept. 7890.

Gutenberg, B. (1957). "Effects of ground on earthquake motion." *Bull. Seism. Soc. Am.*, 47, 221-250.

Hanks, T.C. (1982). "f_{max}." *Bull. Seism. Soc. Am.,* 72, 1867-1879.

Hanks, T.C., and McGuire, R.K. (1981). "The character of high-frequency strong ground motion." *Bull. Seism. Soc. Am.*, 71, 2071-2095.

Hanks, T.C., and Kanamori, H. (1979). "A moment magnitude scale." *J. Geophys. Res.*, 84, 2348-2350.

Hartzell, S.H. (1978). "Earthquake aftershocks as Green's functions." *Geophys. Res. Letters*, 5, 1-4.

Hays, W.W., Rogers, A.M., and King, K.W. (1979). "Empirical data about local ground response." *Proc. Second U.S. Nat. Conf. on Earthq. Engin.*, Earthq. Engin. Res. Inst., 223-232.

Heaton, T.H. (1990). "Evidence for and implications of self-healing pulses of slip in earthquake rupture". *Phys. Earth Planetary Int.*, 64, 1-20.

Hough, S.E., Anderson, J.G. (1988). "High-frequency spectra observed at Anza, California: Implications for Q structure." *Bull. Seism. Soc. Am.*, 78, 692-707.

Hough, S.E., Anderson, J.G., Brune, J., Vernon III, F., Berger, J., Fletcher, J., Haar, L., Hanks, T., and Baker, L. (1988). "Attenuation near Anza, California." *Bull. Seism. Soc. Am.*, 78(2), 672-691.

Houston, H. (1987). "*Source characteristics of large earthquakes at short periods."* Ph.D. Thesis, Calif. Inst. Tech., Pasadena.

Humphrey, J.R., Anderson, J.G., (1992). "Shear-wave attenuation and site response in Guerrero." Submitted to *Bull. Seism. Soc. Am.*

Idriss, I.M., and Seed, H.B. (1968). "Seismic response of horizontal soil layers." *Proc. Am. Soc. Civil Engin.*, *J. Soil Mech. and Found. Div.*, 94, 1003-1031.

Irikura, K. (1983). "Semi-empirical estimation of strong ground motions during large earthquakes." *Bull. Disaster Prevention Res. Inst.*, Kyoto Univ., 33, 63-104.

Joyner, W.B., Warrick, R.E., and Oliver,III, A.A. (1976). "Analysis of seismograms from a downhole array in sediments near San Francisco Bay." *Bull. Seism. Soc. Am.*, 66, 937-958.

Mendez, A.J., and Anderson, J.G. (1991). "The temporal and spatial evolution of the 19 September 1985 Michoacan earthquake as inferred from near-source ground-motion records." *Bull. Seism. Soc. Am.*, 81(3), 844-861.

Mendoza, C., and Hartzell, S.H. (1989). "Slip distribution of the 19 September 1985 Michoacan, Mexico, earthquake: near-source and teleseismic constraints." *Bull. Seism. Soc. Am.*, 79, 655-669.

Murphy, J.R., Davis, A.H., and Weaver, N.L. (1971). "Amplification of seismic body waves by low-velocity surface layers." *Bull. Seism. Soc. Am.*, 61, 109-145.

Ou, G.B., and Herrmann, R.B. (1990). "A statistical model for ground motion produced by earthquakes at local and regional distances." *Bull. Seism. Soc. Am.*, 80, 1397-1417.

Papageorgiou, A.S., and Aki, K. (1983). "A specific barrier model for the quantitative description of inhomogeneous faulting and the prediction of strong ground motion. I. Description of the model." *Bull. Seism. Soc. Am.*, 73, 693-722.

Reid, H.F. (1910). "The California earthquake of April 18, 1906." *The Mechanics of the Earthquake,* Carnegie Inst. of Washington, Publ. 87, 21.

Rogers, A.M., Borcherdt, R.D., Covington, P.A., and Perkins, D.M. (1984). "A comparative ground response study near Los Angeles using recordings of Nevada nuclear tests and the 1971 San Fernando earthquake." *Bull. Seism. Soc. Am.*, 74, 1925-1949.

Schnabel, P.B., Lysmer, J., and Seed, H.B. (1972). "*SHAKE: A computer program for earthquake response analysis of horizontally layered sites.*" Earthq. Engin. Res. Center, Univ. of Calif. at Berkeley, EERC 72-12.

Schneider, J.F., W.J. Silva, and C.L. Stark (1993). Ground motion model for the 1989 **M** 6.9 Loma Prieta earthquake including effects of source, path and site. *Earthquake Spectra,* 9(2), 251-287.

Seed, H.B., Idriss, I.M., and Kiefer, F.W. (1969). "Characteristics of rock motions

during earthquakes." *J. Soil Mech. Found. Div.*, Am. Soc. Civil Engin., ASCE, 95(SM5).

Silva, W.J., N. Abrahamson, G. Toro and C. Costantino. (1997). "Description and validation of the stochastic ground motion model." Report Submitted to Brookhaven National Laboratory, Associated Universities, Inc. Upton, New York 11973, Contract No. 770573.

Silva, W.J. and Darragh, R.B. (1995). "Engineering characterization of strong ground motion recorded at rock sites." Draft Final Report Submitted to Electric Power Res. Inst., EPRI RP 2556-48.

Silva, W.J. and Stark, C.L. (1992). "Source, path, and site ground motion model for the 1989 M 6.9 Loma Prieta earthquake." CDMG draft final report.

Silva, W.J. (1991). "Global characteristics and site geometry." *Proceedings: NSF/EPRI Workshop on Dynamic Soil Properties and Site Characterization.* Electric Power Res. Inst., EPRI NP-7337.

Silva, W.J., Darragh, R.B., and Wong, I.G. (1990). "Engineering characterization of earthquake strong ground motions with applications to the Pacific Northwest." in Hays, W.W., ed., *Proceedings of the Third NEHRP Workshop on earthquake Hazards in the Puget sound/Portland region*, U.S. geological Survey Open-File report (in press).

Silva, W.J., Darragh, R.B., Green, R.K., and Turcotte, F.T. (1989). *Estimated Ground Motions for a new madrid Event.* U.S. Army Engineer Waterways Experiment Station, Wash., DC, Misc. Paper GL-89-17.

Silva, W.J., and Lee, K. (1987). "*WES RASCAL code for synthesizing earthquake ground motions.*" State-of-the-Art for Assessing Earthquake Hazards in the United States, Report 24, U.S. Army Engineers Waterways Experiment Station, Misc. Paper S-73-1.

Silva, W.J., (1976). "Body waves in a layered anelastic solid." *Bull. Seism. Soc. Am.*, 66(5), 1539-1554.

Toro, G.R., and McGuire, R.K. (1987). "An investigation into earthquake ground motion characteristics in eastern North America." *Bull. Seism. Soc. Am.*, 77, 468-489.

Tucker, B.E., King, J.L. (1984). "Dependence of sediment-filled valley response on the input amplitude and the valley properties." *Bull. Seism. Soc. Am.*, (74), 153-165.

Wells, D.L., Coppersmith, K.J. (1993). "Updated empirical relationships among magnitude, rupture length, rupture area, and surface displacement". Submitted to *Bull. Seism. Soc. Am.*

Wiggins, J.H. (1964). "Effects of site conditions on earthquake intensity." *J. Structural Div., Proc.*, Am. Soc. Civil Engin., ASCE 90(2), Part I.

Wood, H.O. (1908). "Distribution of apparent intensity in San Francisco, in the California earthquake of April 18, 1906." *Report of the State Earthquake Investigation Commission*, Wash., D.C.: Carnegie Institute, 1, 220-245.

TABLE 1

MICHOACAN MODELING
SITES AND KAPPA VALUES

Name	Label	Kappa(sec)	Site Function
Caleto de Campos	CMP	0.045[1]	
La Villita	VIL	0.100[1]	
La Union	UNI	0.045[1]	
Zihuatanejo	ZIH	0.050[1]	
Papanoa	PPN	0.020[1]	*
El Suchil	SUC	0.040[2]	
Atoyac	ATO	0.028[2]	
El Paraiso	PAR	0.024[2]	*
El Cayaco	CAY	0.036[2]	*
Coyuca	CYC	0.036[2]	
Teacalco	TEA	0.049[2]	*
El Ocotito	OTT	0.027[2]	*
Cerro de Piedro	CDP	0.038	*
Las Mesas	MES	0.021[2]	

[1] From Silva and Darragh, (1993)
[2] From Humphrey and Anderson (1993)

Table 2

VALPARISO MODELING
SITES AND KAPPA VALUES

Name	Label	Kappa (sec)
Valpariso UTFSM	VALU	0.040[1]
Zapallar	ZAP	0.020[1]
Papudo	PAP	0.020[1]
Los Vilos	LVI	0.060[1]
Pichilemu	PIC	0.040[1]
Constitucion	CNS	0.040[1]

[1] Based on template fits to response spectral shapes.

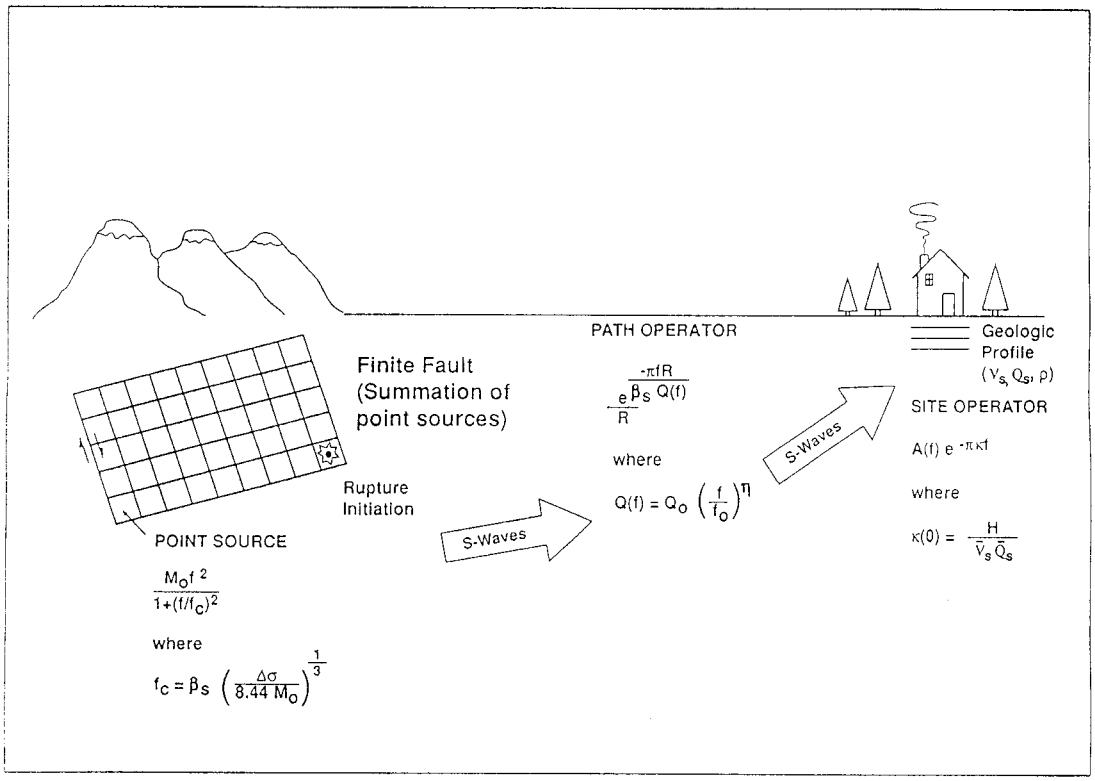

Figure 1. Schematic of ground motion model.

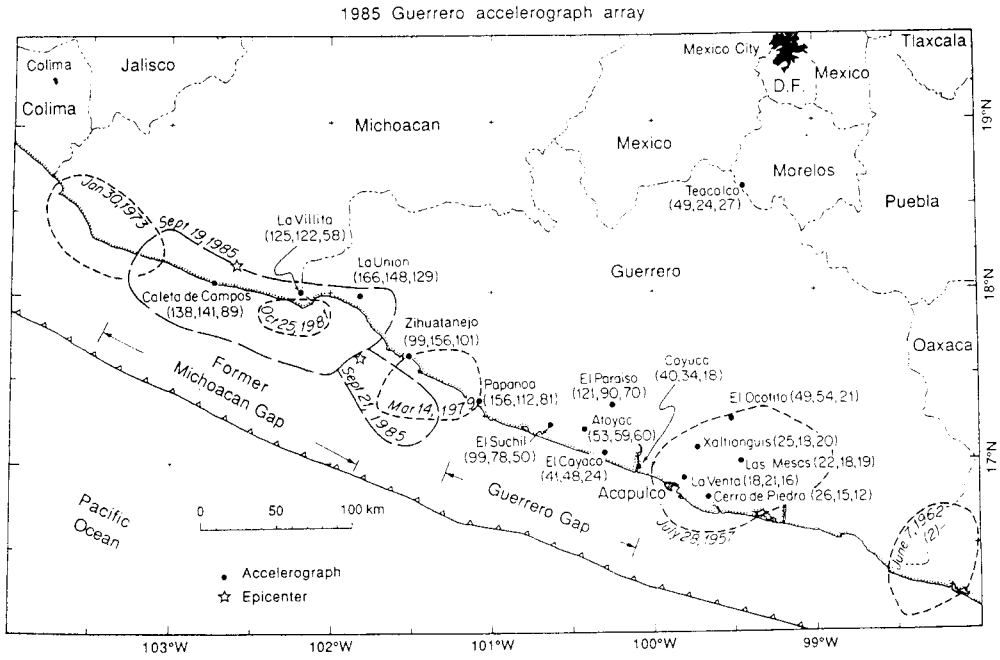

Figure 2. Map of coastal Mexico, epicenters and aftershock zones of 1985 events, and locations of strong motion stations in Guerrero array on 19 September 1985. Short dashed lines show limits of aftershocks of large earthquakes in this region since 1951. Peak accelerations (cm/sec^2) are given for each station for the north, east, and vertical components, respectively, in parentheses (Source: Anderson et al., 1986).

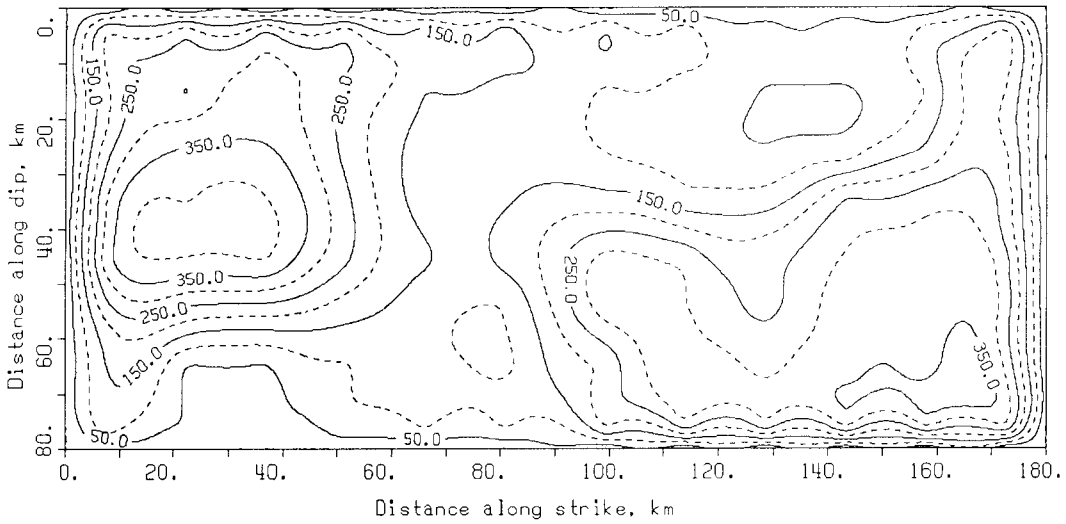

Figure 3. Slip model of the September 19, 1985 M 8.03 Michoacan, Mexico earthquake (Mendoza and Anderson, 1991).

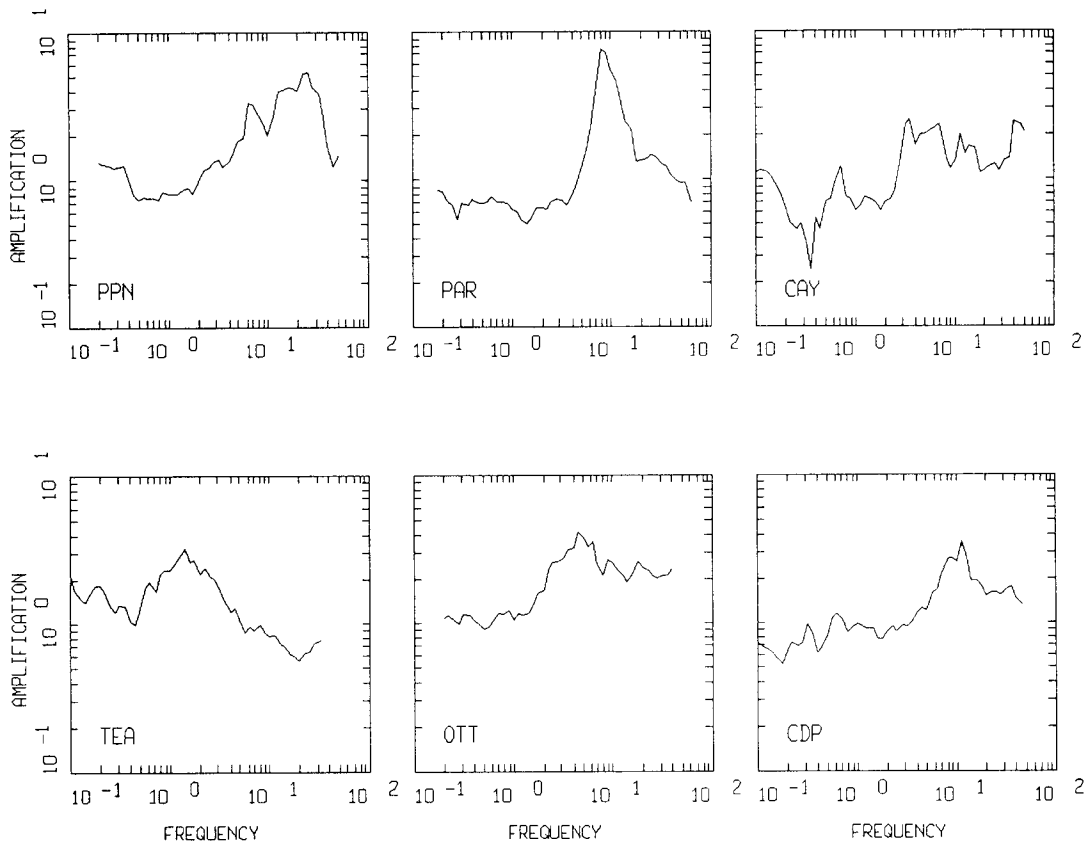

Figure 4. Site amplification factors available for six of the fourteen sites of the Guerrero accelerograph array which were modeled (see Table 1 for site names and Figure 2 for site locations).

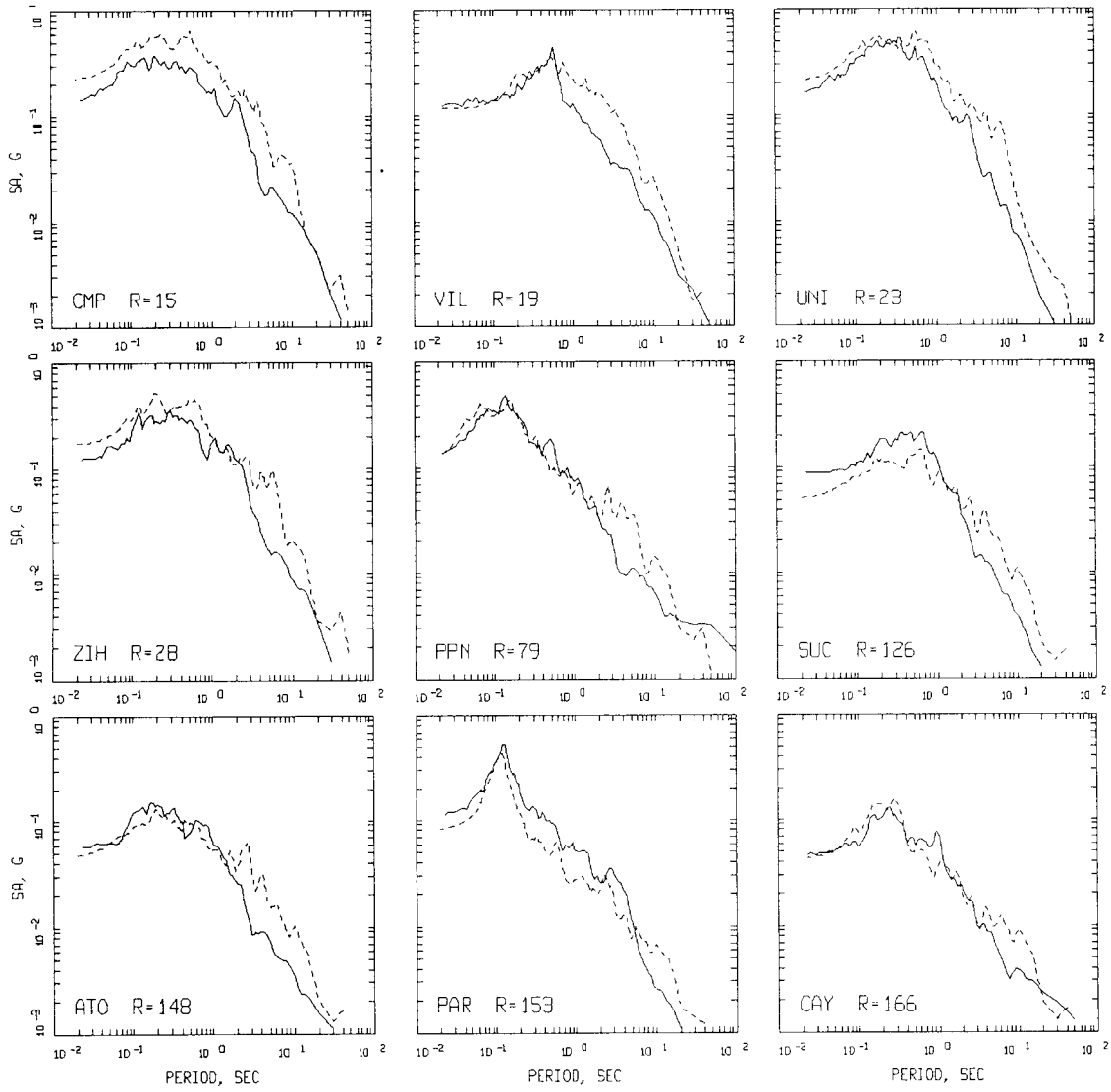

Figure 5. Comparison of 5% damped acceleration response spectra computed for the Michoacan, Mexico earthquake (dashed line) to average of the two horizontal components computed from the recorded motions (solid lines) at fourteen rock sites.

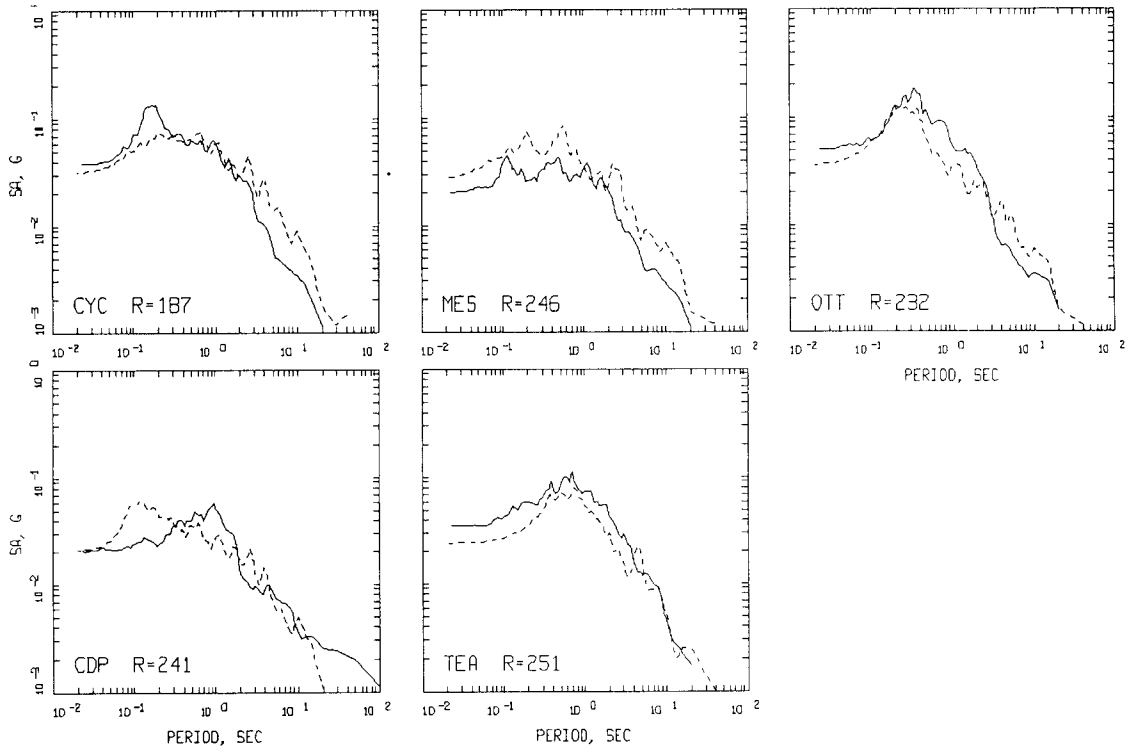

Figure 5. (continued)

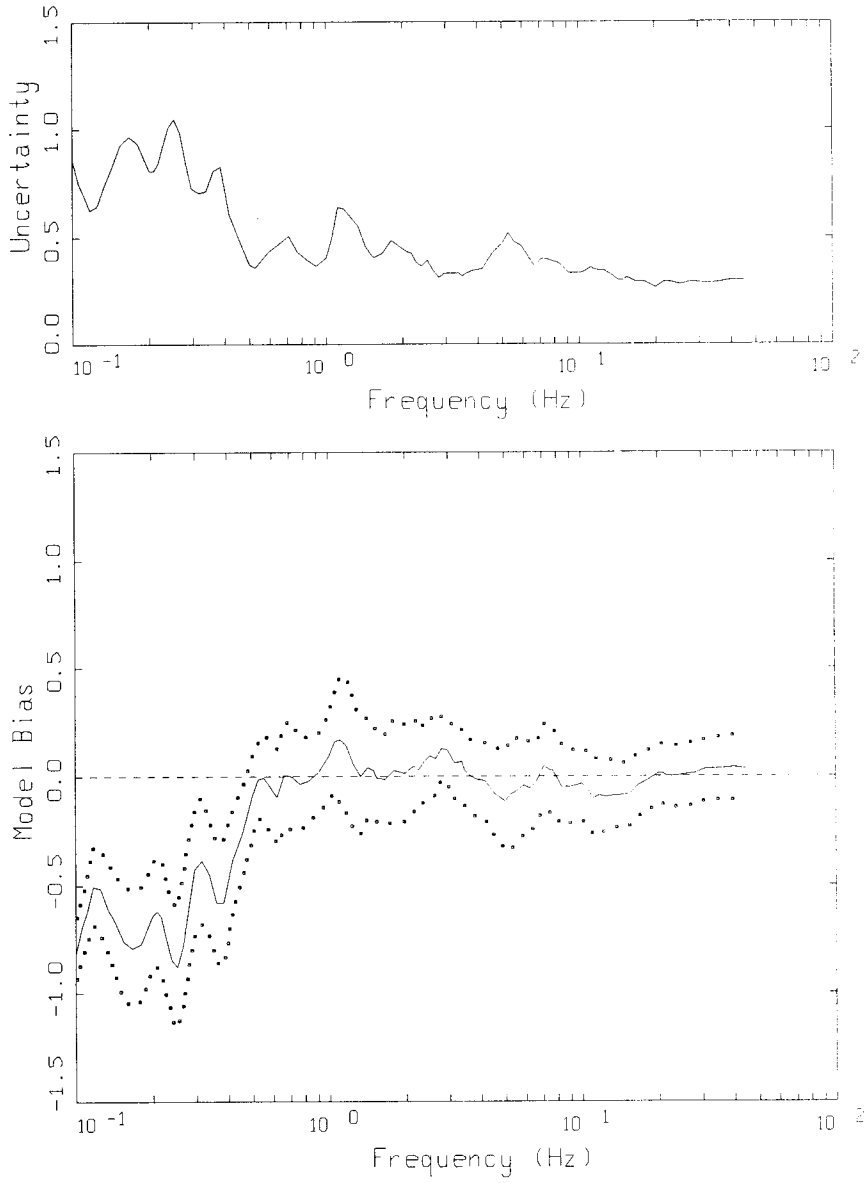

Figure 6. Modeling uncertainty (σ_{ln}) (upper) and model bias with 90% confidence limits (lower) computed for the Michoacan, Mexico earthquake.

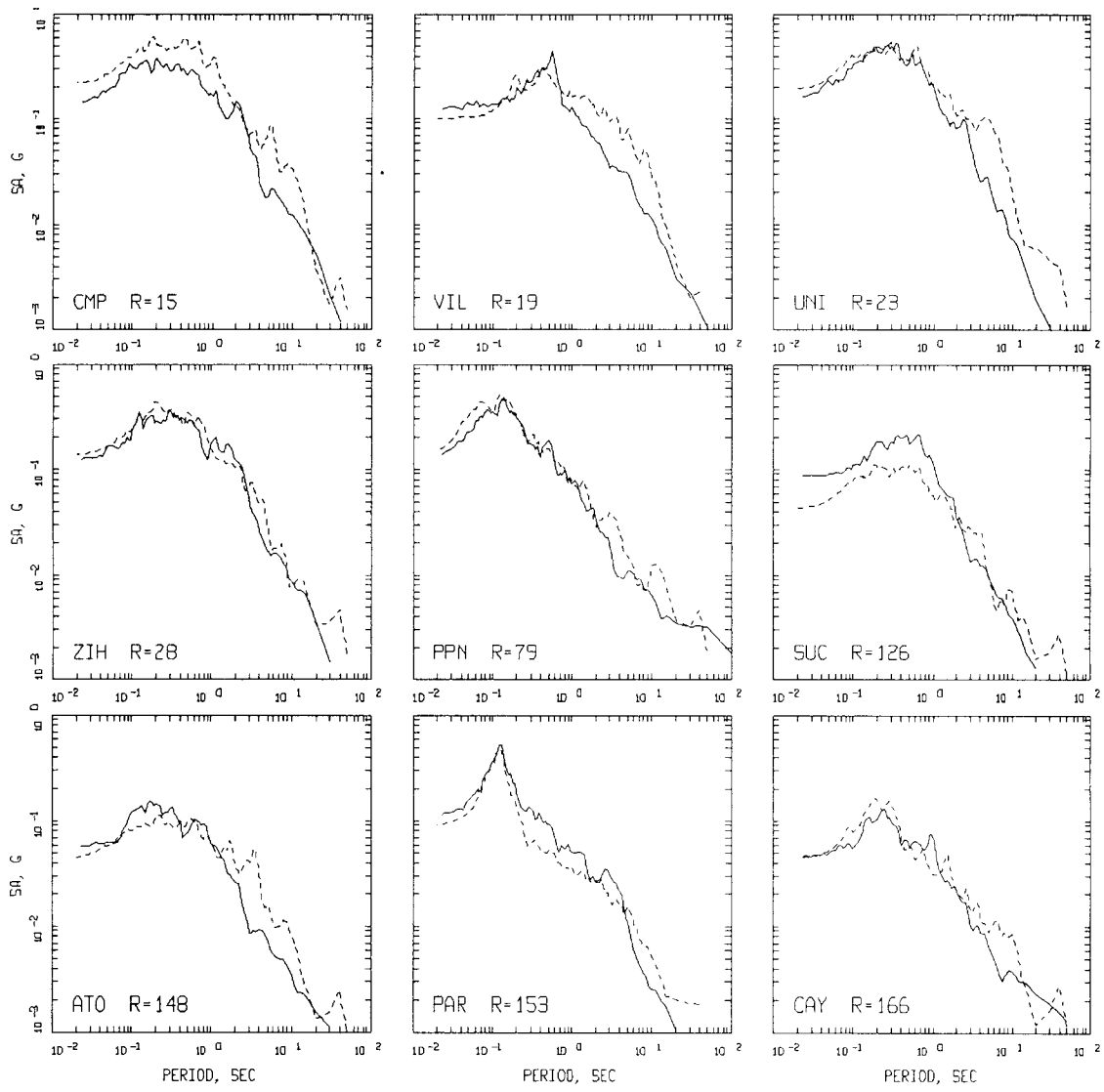

Figure 7. Comparison of 5% damped acceleration response spectra computed for the Michoacan, Mexico earthquake (dashed line) modeling the effects of direct waves plus post-critically reflected waves to average of the two horizontal components computed from the recorded motions (solid lines) at fourteen rock sites.

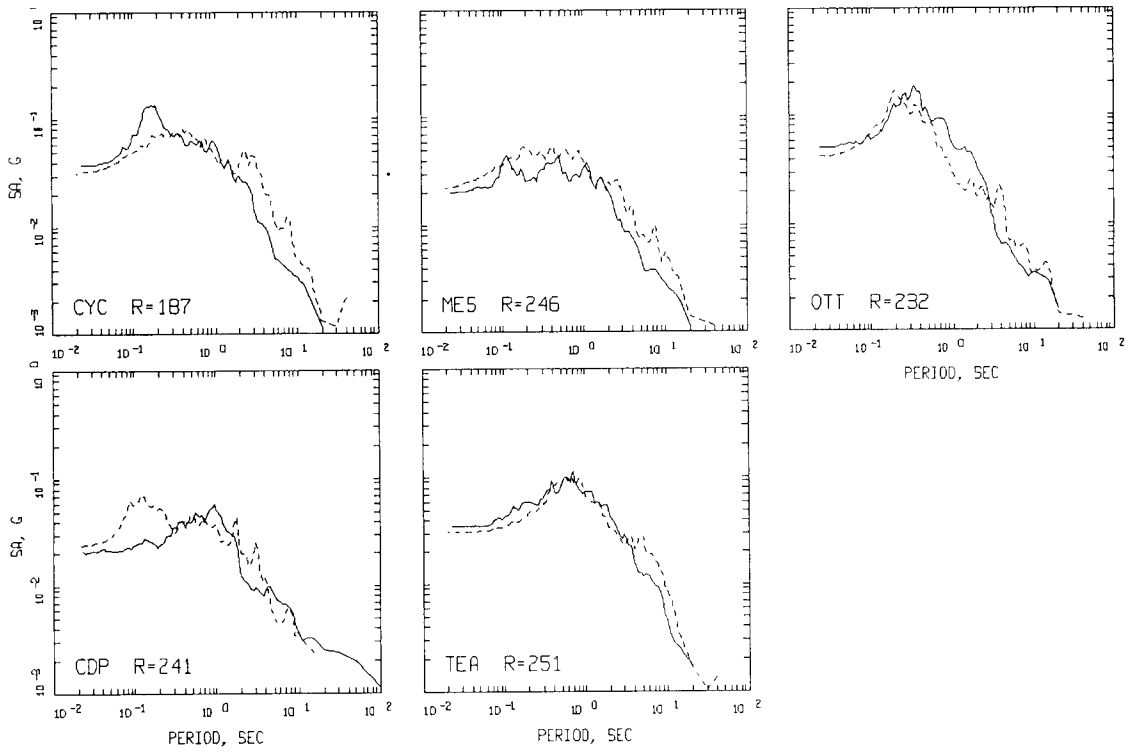

Figure 7. (continued)

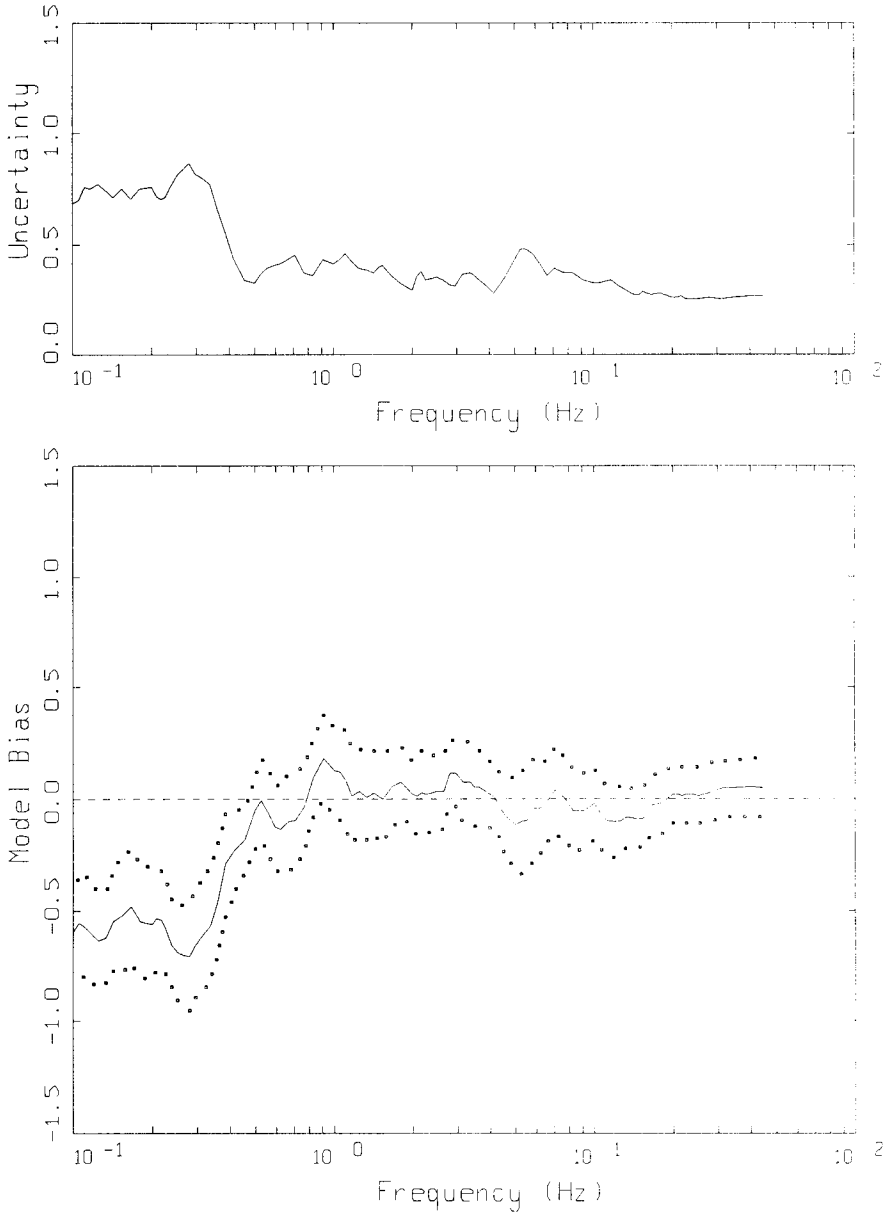

Figure 8. Modeling uncertainty (σ_{ln}) upper and model bias with 90% confidence limits (lower) computed for the Michoacan, Mexico earthquake. Model predictions include the effects of direct waves plus post-critical reflections.

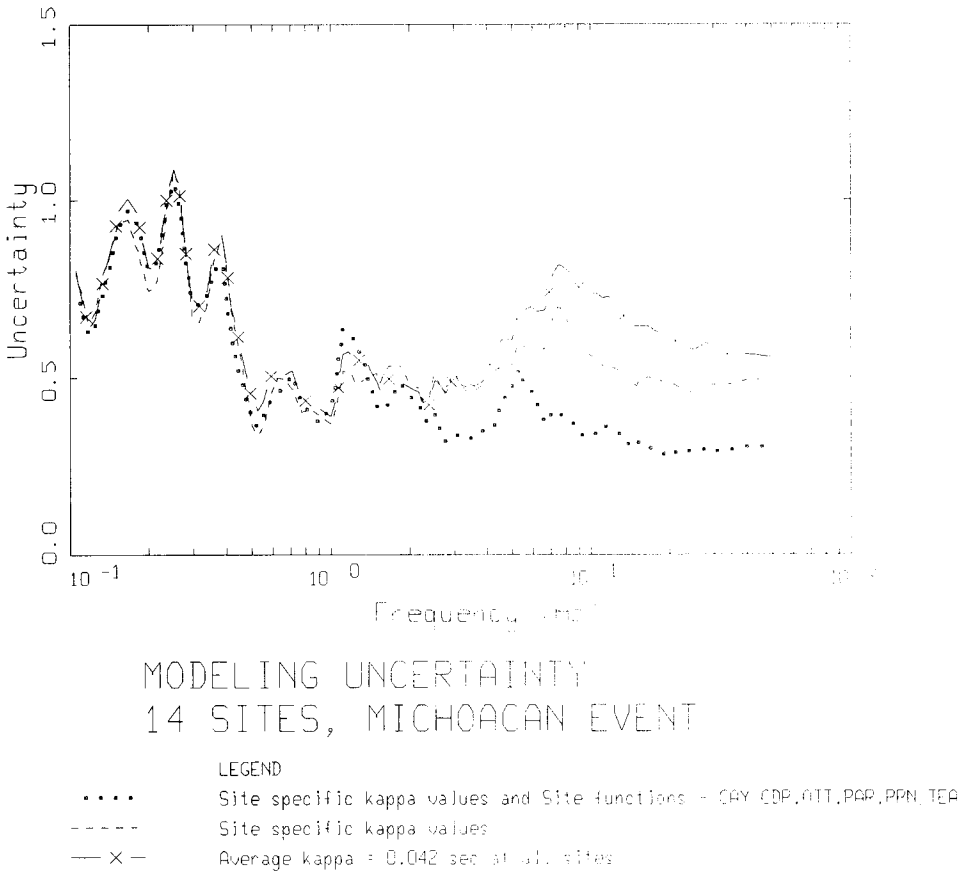

Figure 9. Comparison of modeling uncertainty computed using site functions and site specific kappa values (dotted line, same as Figure 6), without site functions but retaining site specific kappa values (dashed line), without site functions and with a constant average kappa value of 0.042 sec (crosses).

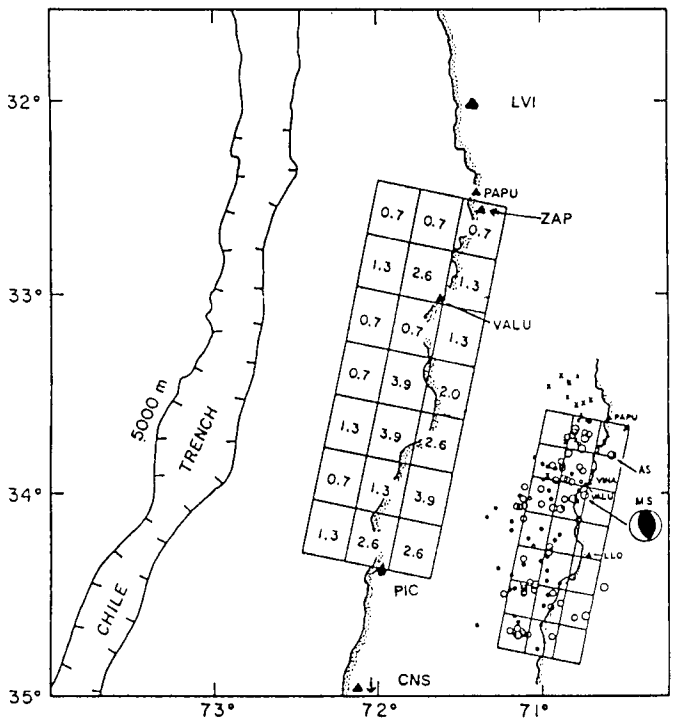

Figure 10. Slip model (Somerville et al., 1990) and station locations for the March 3, 1985 Valpariso M 7.93 earthquake.

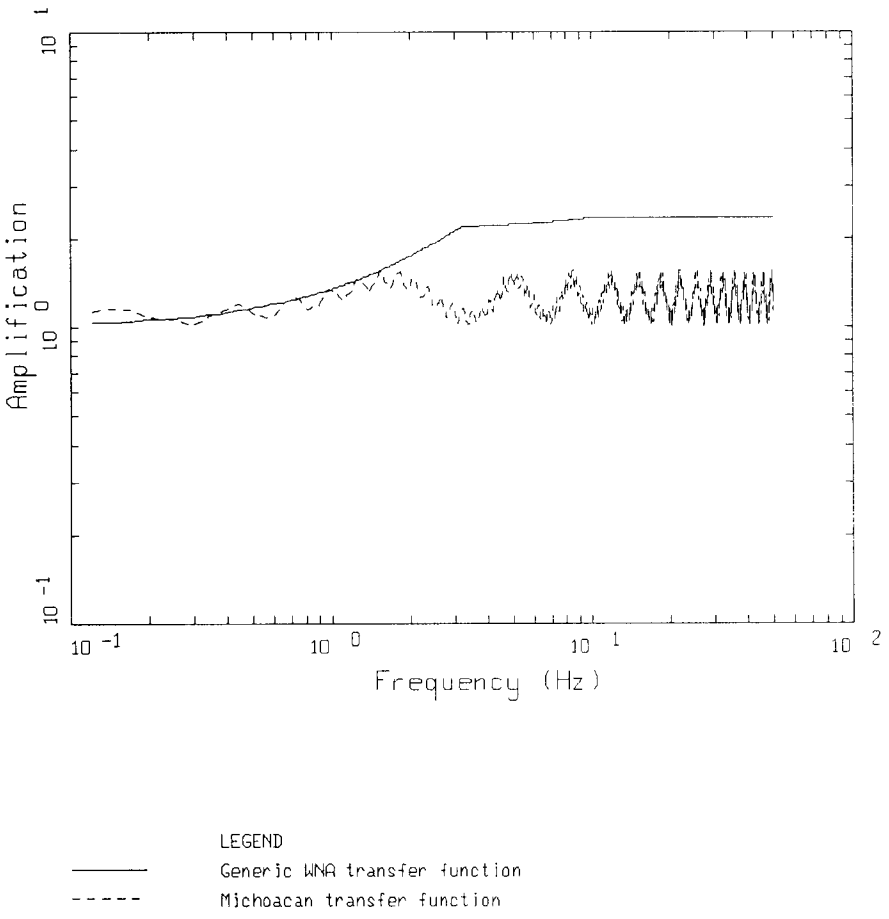

Figure 11. Comparison of crustal amplification for generic western North America (Boore, 1986) with that computed for the crustal structure of the Guerrero array.

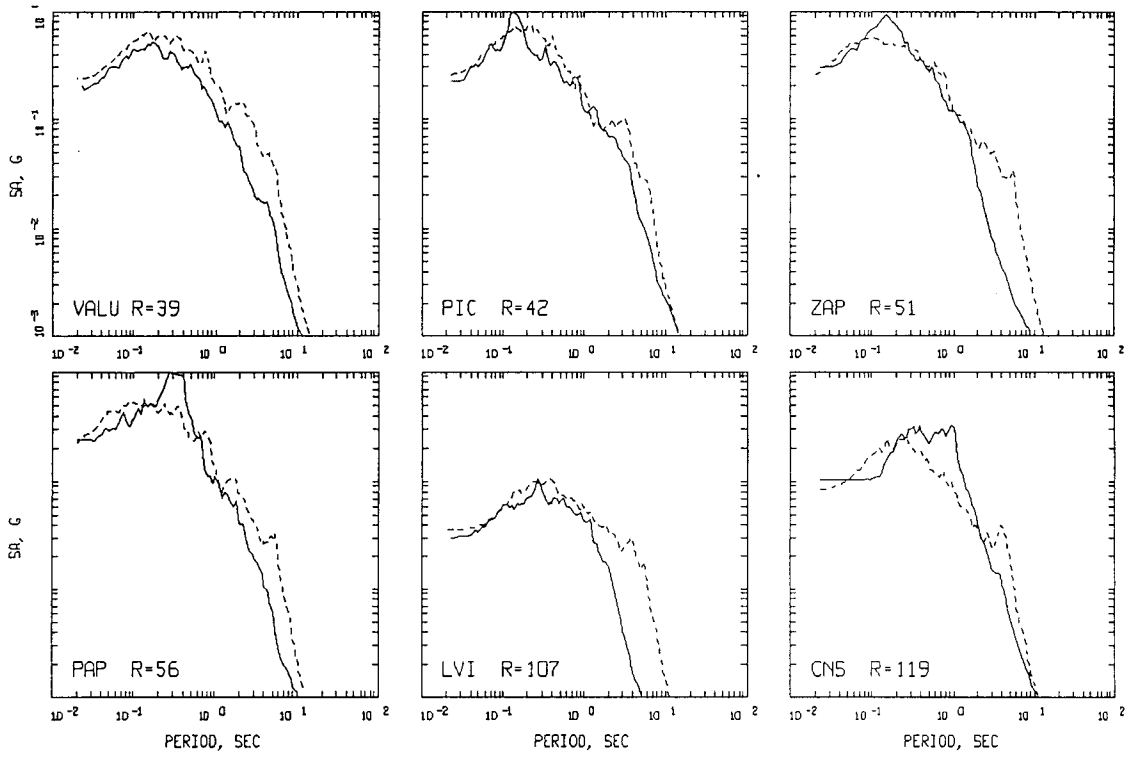

Figure 12. Comparison of 5% damped acceleration response spectra computed for the Valpariso, Chile earthquake (dashed line) to average of the two horizontal components computed from the recorded motions (solid lines) at six rock sites.

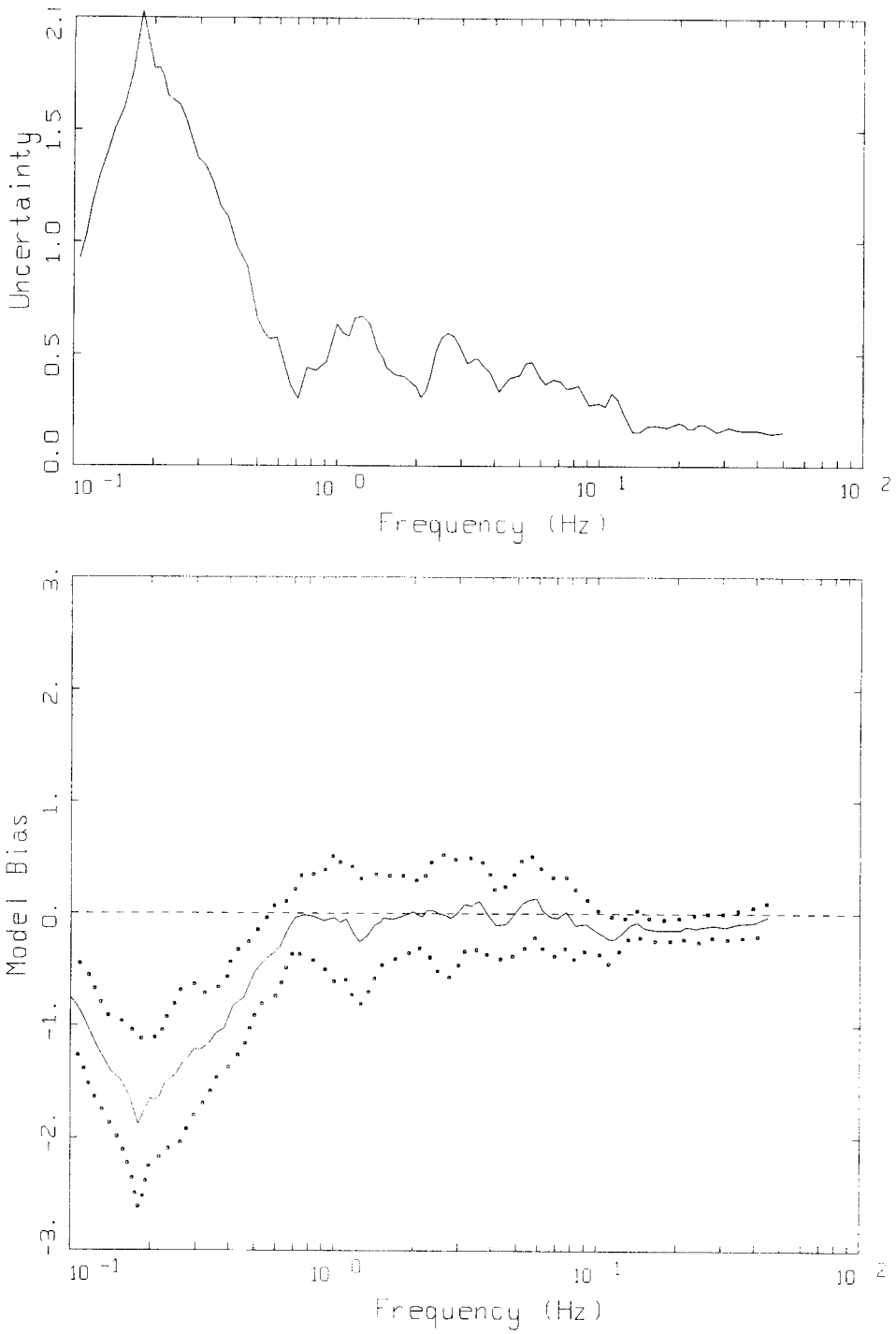

Figure 13. Modeling uncertainty (σ_{ln}) (upper) and model bias with 90% confidence limits (lower) computed for the Valpariso, Chile earthquake.

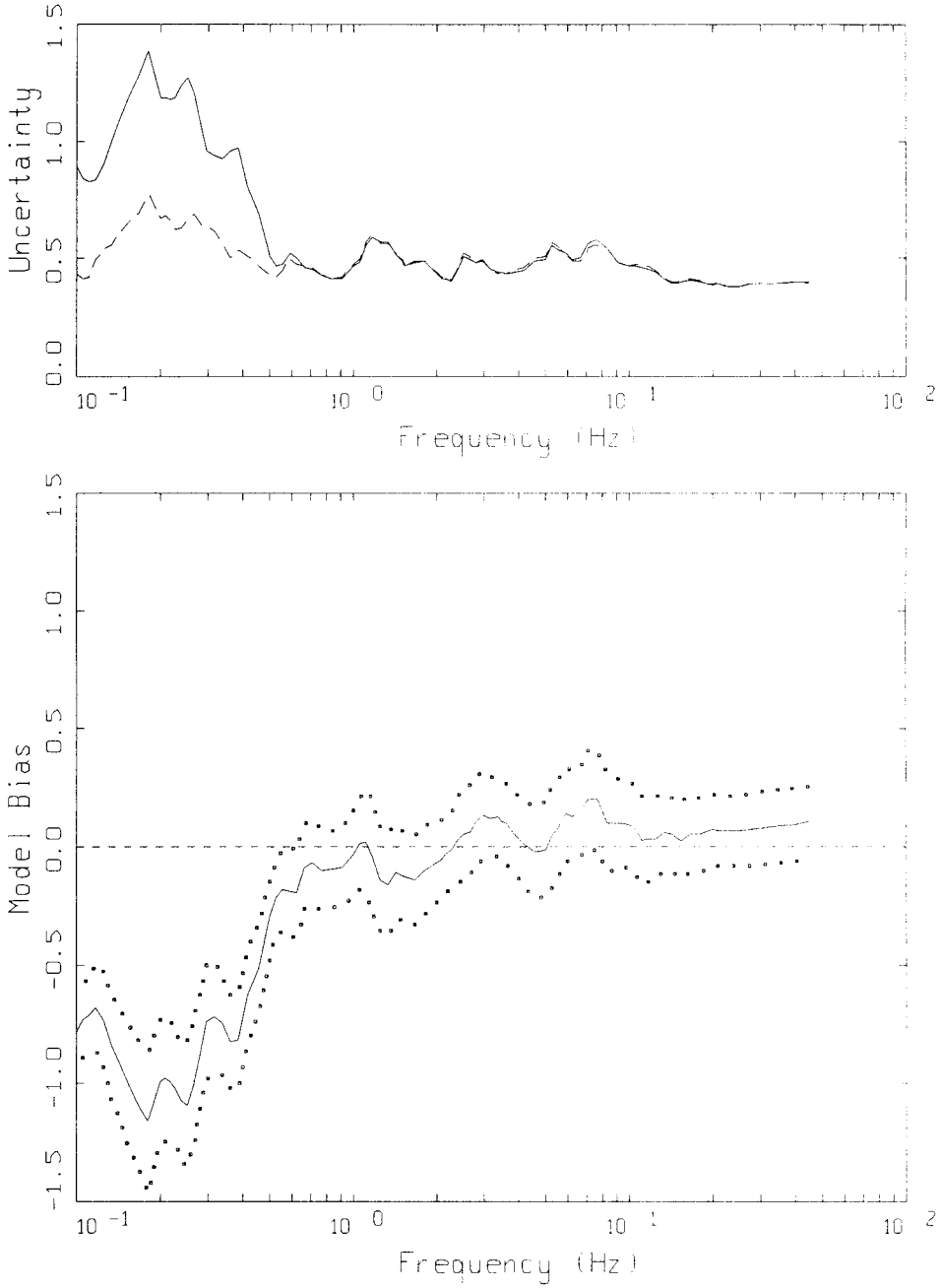

Figure 14. Modeling uncertainty (solid) and bias corrected modeling uncertainty (dashed) (both σ_{ln}) (upper) and model bias with 90% confidence limits (lower) computed for both the Michoacan, Mexico and Valpariso, Chile earthquakes.